

## Wakefield in a waveguide

Y. P. Bliokh, J. G. Leopold, G. Shafir, A. Shlapakovski, and Ya. E. Krasik  
 Physics Department, Technion, Haifa 32000, Israel

(Received 20 January 2017; accepted 15 May 2017; published online 26 June 2017)

The feasibility of an experiment which is being set up in our plasma laboratory to study the effect of a wakefield formed by an ultra-short ( $\leq 10^{-9}$  s) high-power ( $\sim 1$  GW) microwave (10 GHz) pulse propagating in a cylindrical waveguide filled with an under-dense [ $(2-5) \times 10^{10} \text{ cm}^{-3}$ ] plasma is modeled theoretically and simulated by a particle in cell code. It is shown that the radial ponderomotive force plays a circular key role in the wakefield formation by the TM mode waveguide. The model and the simulations show that powerful microwave pulses produce a wakefield at lower plasma density and electric field gradients but larger space and time scales compared to the laser produced wakefield in plasmas, thus providing a more accessible platform for the experimental study. *Published by AIP Publishing.* [<http://dx.doi.org/10.1063/1.4989731>]

### I. INTRODUCTION

The excitation of space-charge oscillations in under-dense plasmas by an ultra-short pulse of intense laser electromagnetic radiation resulting in a wakefield formation is perhaps the most noticeable example of a wave-plasma interaction. This physical phenomenon, being interesting by itself, holds the greatest promise for charged particles acceleration to the GeV range of energy within a distance of  $\leq 10^{-3}$  m.<sup>1-4</sup> The maximal accelerating electric field of plasma oscillations excited by the electromagnetic pulse grows with the plasma density. In order to exceed significantly the accelerating fields realized in traditional accelerators ( $\leq 100$  MV/m), the plasma density should be, on the one hand, large enough. On the other hand, the frequency of the electromagnetic pulse should exceed the plasma electron frequency. The laser pulses are best suited for wakefield acceleration: modern lasers produce sufficiently powerful ( $\sim 10^{19}$  W/cm<sup>2</sup>) and short ( $\sim 10^{-13}$  s) pulses which can excite wakefields of large amplitude ( $\geq 10^{11}$  V/m) in dense ( $\sim 10^{19}$  cm<sup>-3</sup>) plasmas. Thus, the laser pulse driving wakefields are characterized by small temporal and spatial scales ( $\leq 10^{-2}$  cm) that make experiments investigating the underlying physical processes challenging.

Wakefield excitation can be studied by applying an ultra-short high power microwave (HPM) pulse interacting with the plasma.<sup>5</sup> Similar to the case of the ponderomotive field excitation in plasmas by powerful laser pulses, the density modulation and wakefields will be generated most efficiently when the microwave pulse duration  $t_p$  will be approximately equal to the half of the plasma oscillation period, i.e.,  $\omega_{pe} t_p \approx \pi$ , where  $\omega_{pe}$  is the plasma electron frequency. For instance, for the microwave pulse duration of  $\sim 0.35$  ns, the optimal plasma electron density is  $\sim 2.5 \times 10^{10} \text{ cm}^{-3}$ . It is clear that in this case, the expected wakefield's amplitude will be several orders lower than those excited by powerful and ultrashort laser pulses. However, wakefield excitation by hundreds of MW power microwave pulse at  $\sim 10$  GHz frequency and a duration of  $\sim 1$  ns in a plasma with the density in the range of  $10^{10}$ – $10^{11} \text{ cm}^{-3}$  is characterized by the significantly larger temporal and spatial scales. This allows the application of different time- and space-resolved diagnostics of the plasma

parameters, which determine formation and evolution of the wakefield, and the comparison between experimental and simulations results. Fast progress in generation of short duration microwave pulses with the power of several GW (Ref. 6) makes reasonable to use such pulses for detailed investigation of wakefield excitation and evolution.

Recently, there is interest in the excitation of wakefields by electromagnetic pulses with more complex than linear or circular polarization and transversal profiles different from Gaussian. In particular, wakefields excited by a pulse of the TE mode of a rectangular waveguide filled with plasmas were considered in Refs. 7–12. For instance, one can expect a wakefield of  $\sim 10$  kV/cm in the case of the TE mode microwave pulse with a power density of  $0.25 \text{ MW/cm}^2$  and a frequency of  $\sim 5$  GHz propagating in a rectangular waveguide filled by plasmas with a density of  $\sim 3 \times 10^9 \text{ cm}^{-3}$ .<sup>7</sup> The field structure of the driving electromagnetic pulse in a waveguide differs strongly from the one in the unbounded plasma. Moreover, the electromagnetic energy is concentrated not only in a single focal region, as in the case of the unbounded plasma, but in a small transversal cross-sectional area along the entire waveguide. These characteristics can also simplify the experimental diagnostics of the plasma parameters.

In this paper, the wakefield excitation by an HPM pulse of a TM mode propagating in a cylindrical waveguide filled with plasmas is studied analytically and numerically. It is shown that the radial component of the ponderomotive force, caused by the radial structure of TM mode, exceeds considerably the longitudinal component, relating to the temporal evolution of the pulse envelope. Waveguides with walls partially transparent to the plasma particles flux, as it is planned in our experimental setup, are considered along with waveguides with non-transparent conducting walls. Other experimental variations are also numerically modeled.

### II. BASIC EQUATIONS

The backward wave oscillator (BWO) operating in the super-radiant regime<sup>13,14</sup> is one of the best suited devices for the generation of short HPM pulses. The slow-wave structure of the BWO consists of a cylindrical waveguide with

periodically corrugated conducting walls. In order to study the interaction of the electromagnetic pulse with under-dense plasmas, it seems reasonable to connect the output end of the BWO with a smooth cylindrical waveguide of the same diameter filled with a preliminarily formed under-dense plasma. This design allows one to eliminate interface insulators and transition elements (for instance, mode converter) and reduce the power losses caused by these elements. The electromagnetic mode propagating through the plasma is the same as the BWO's operating mode, namely,  $\text{TM}_{01}$  mode, whose electric and magnetic fields are  $E_z$ ,  $E_r$ , and  $H_\phi$

$$E_z = -\frac{k_\perp}{k_z} E_0(z, t) J_0(k_\perp r) \cos(\omega t - k_z z), \quad (1a)$$

$$E_r = E_0(z, t) J_1(k_\perp r) \sin(\omega t - k_z z), \quad (1b)$$

$$H_\phi = \frac{k_0}{k_z} E_0(z, t) J_1(k_\perp r) \sin(\omega t - k_z z). \quad (1c)$$

Here,  $k_0 = \omega/c = \sqrt{k_z^2 + k_\perp^2}$ ,  $k_\perp = \gamma_{0,1}/R$ ,  $\gamma_{0,1} \approx 2.4$  is the first zero of the Bessel function  $J_0$ , and  $R$  is the waveguide radius. Equation (1) describes a wave packet (pulse), when the amplitude  $E_0$  is a slowly varying function of the argument  $t - z/v_g$ , where  $v_g = d\omega/dk_z = ck_z/k_0$  is the wave group velocity. Electron motion in the fields of the  $\text{TM}_{01}$  wave is described by the following equations:

$$\frac{dv_z}{dt} = \frac{e}{m} E_z + \frac{e}{mc} v_r H_\phi, \quad (2a)$$

$$\frac{dv_r}{dt} = \frac{e}{m} E_r - \frac{e}{mc} v_z H_\phi, \quad (2b)$$

$$\frac{dz}{dt} = v_z, \quad (2c)$$

$$\frac{dr}{dt} = v_r. \quad (2d)$$

It is assumed in Eq. (2) that the amplitude of the electric field is small enough, so that the dimensionless amplitude  $\mathcal{E} = \frac{eE_0}{mc\omega} \ll 1$ , which corresponds to the non-relativistic electron motion.

Let us introduce dimensionless variables  $\tau = \omega t$ ,  $\xi = k_z z$ ,  $\rho = k_\perp r$ ,  $\beta_\xi \equiv d\xi/d\tau = k_z v_z/k_0 c$ , and  $\beta_\rho \equiv d\rho/d\tau = k_\perp v_r/k_0 c$ .

Now, Eq. (2) reads as

$$\begin{aligned} \frac{d\beta_\xi}{d\tau} &= -\sin\psi \mathcal{E}(\theta) J_0(\rho) \cos(\tau - \xi) \\ &+ \frac{1}{\sin\psi} \mathcal{E}(\theta) J_1(\rho) \sin(\tau - \xi) \beta_\rho, \end{aligned} \quad (3a)$$

$$\begin{aligned} \frac{d\beta_\rho}{d\tau} &= \sin\psi \mathcal{E}(\theta) J_1(\rho) \sin(\tau - \xi) \\ &- \frac{\sin\psi}{\cos^2\psi} \mathcal{E}(\theta) J_1(\rho) \sin(\tau - \xi) \beta_\xi, \end{aligned} \quad (3b)$$

$$\frac{d\xi}{d\tau} = \beta_\xi, \quad (3c)$$

$$\frac{d\rho}{d\tau} = \beta_\rho. \quad (3d)$$

Here,  $\sin\psi = k_\perp/k_0$ ,  $\cos\psi = k_z/k_0 = v_g/c$ , and  $\theta = \tau - \xi/\cos^2\psi$ . We should bear in mind that the wave amplitude  $\mathcal{E}(\theta)$  is a slowly varying function, i.e.,  $\mathcal{E}^{-1} d\mathcal{E}/d\theta \propto \tau_p^{-1} \ll 1$ , where  $\tau_p = \omega t_p \gg 1$  and  $t_p$  is the pulse duration.

### III. FAST AND SLOW ELECTRON MOTION

The right-hand sides of Eq. (3) contain two time scales: fast oscillating functions  $\cos(\tau - \xi)$  and  $\sin(\tau - \xi)$  and the slowly varying function  $\mathcal{E}(\theta)$ . Correspondingly, the solutions for the axial  $\xi(\tau)$  and the radial  $\rho(\tau)$  motion of electrons are two-scale functions:  $\xi = \bar{\xi} + \tilde{\xi}$  and  $\rho = \bar{\rho} + \tilde{\rho}$ , where the mark  $\bar{(\cdot)}$  means the average over the fast oscillations and the mark  $\tilde{(\cdot)}$  indicates the oscillating part. The oscillating parts are proportional to  $\mathcal{E}$ , while the slow-varying parts are proportional to  $\mathcal{E}^2 \ll \mathcal{E}$ . Below, we will neglect the terms which contain  $(d\mathcal{E}/d\theta)^2$ ,  $\mathcal{E} d^2\mathcal{E}/d\theta^2$ , and higher derivatives of  $\mathcal{E}$ .

The oscillating parts of the solution of Eq. (3) are

$$\tilde{\beta}_\xi = -\sin\psi J_0(\bar{\rho}) \left[ \mathcal{E}(\bar{\theta}) \sin(\tau - \bar{\xi}) + \frac{d\mathcal{E}}{d\theta} \cos(\tau - \bar{\xi}) \right], \quad (4a)$$

$$\tilde{\xi} = \sin\psi J_0(\bar{\rho}) \left[ \mathcal{E}(\bar{\theta}) \cos(\tau - \bar{\xi}) - 2 \frac{d\mathcal{E}}{d\theta} \sin(\tau - \bar{\xi}) \right], \quad (4b)$$

$$\tilde{\beta}_\rho = -\sin\psi J_1(\bar{\rho}) \left[ \mathcal{E}(\bar{\theta}) \cos(\tau - \bar{\xi}) - \frac{d\mathcal{E}}{d\theta} \sin(\tau - \bar{\xi}) \right], \quad (4c)$$

$$\tilde{\rho} = -\sin\psi J_1(\bar{\rho}) \left[ \mathcal{E}(\bar{\theta}) \sin(\tau - \bar{\xi}) + 2 \frac{d\mathcal{E}}{d\theta} \cos(\tau - \bar{\xi}) \right]. \quad (4d)$$

The slowly varying function  $\bar{\beta}_\xi$  is defined by the equation

$$\begin{aligned} \frac{d\bar{\beta}_\xi}{d\tau} &= -\sin\psi \langle \mathcal{E}(\theta) J_0(\rho) \cos(\tau - \xi) \rangle \\ &+ \frac{1}{\sin\psi} \mathcal{E}(\bar{\theta}) J_1(\bar{\rho}) \langle \sin(\tau - \bar{\xi}) \tilde{\beta}_\rho \rangle, \end{aligned} \quad (5)$$

where  $\langle \dots \rangle$  means averaging over the fast oscillations. Using the expansions

$$\begin{aligned} \mathcal{E}(\theta) &\approx \mathcal{E}(\bar{\theta}) - \frac{\tilde{\xi}}{\cos^2\psi} \frac{d\mathcal{E}(\bar{\theta})}{d\theta}, \\ J_0(\rho) &\approx J_0(\bar{\rho}) - J_1(\bar{\rho}) \tilde{\rho}, \\ \cos(\tau - \xi) &\approx \cos(\tau - \bar{\xi}) + \tilde{\xi} \sin(\tau - \bar{\xi}). \end{aligned}$$

One can present Eq. (5) for the axial electron motion as follows:

$$\begin{aligned} \frac{d\bar{\beta}_\xi}{d\tau} &= \frac{1}{2} \left[ \sin^2\psi \left( 1 + \frac{1}{2\cos^2\psi} \right) J_0^2(\bar{\rho}) \right. \\ &\left. + \left( \frac{1}{2} - \sin^2\psi \right) J_1^2(\bar{\rho}) \right] \frac{d\mathcal{E}^2(\bar{\theta})}{d\theta}. \end{aligned} \quad (6a)$$

Similarly, one can obtain an equation for the radial motion

$$\frac{d\bar{\beta}_\rho}{d\tau} = \frac{1}{2} \sin^2\psi \mathcal{E}^2(\bar{\theta}) \left[ \left( \frac{1}{\cos^2\psi} - 2 \right) J_0(\bar{\rho}) + \frac{1}{\rho} J_1(\bar{\rho}) \right] J_1(\bar{\rho}). \quad (6b)$$

Equations (6a) and (6b), supplemented with equations

$$\frac{d\bar{\xi}}{d\tau} = \bar{\beta}_\xi \quad (6c)$$

and

$$\frac{d\bar{\rho}}{d\tau} = \bar{\beta}_\rho, \quad (6d)$$

form the complete set, which describe the motion of a single electron.

#### IV. SPACE CHARGE FIELD

The right-hand sides of Eqs. (6a) and (6b) represent the forces experienced by the electron in the longitudinal and radial directions, respectively. The longitudinal force is proportional to  $d\mathcal{E}^2/d\theta \propto \tau_p^{-1}\mathcal{E}^2$ . In contrast, the radial force does not contain a derivative of  $\mathcal{E}^2$ .

When the waveguide radius is of the same order of magnitude as the wavelength, i.e.,  $\sin\psi \approx 1$ , the longitudinal force exceeds the radial one near the axis only, where  $\rho \approx \tau_p^{-1} \ll 1$ . Moreover, the longitudinal force as a function of time changes its sign, while the radial force remains always positive. It means that the electromagnetic pulse shifts almost all electrons in the waveguide cross-section mainly in the radial direction. Note that in a super-dimensional waveguide ( $\sin\psi \rightarrow 0$ ), the longitudinal force dominates.

Until now, the motion of a single electron was considered. Let the waveguide be filled by a low-density plasma,  $\omega_p \ll \omega$ , where  $\omega_p$  is the electron Langmuir frequency. The microwave pulse pushes out plasma electrons in the radial direction away from the axis. The space charge of the plasma ions (considered as motionless) produces a radial electric field which attracts the electrons to the axis. The axial electric field of the space charge can be neglected due to the reasons explained above. Moreover, the characteristic spatial scale of the longitudinal modulation of the electron density is of the order of the pulse length  $v_g t_p$ . Because this length is much larger than the waveguide radius, the radial electric field caused by this longitudinal modulation is much stronger than the axial one. Therefore, only the radial component  $E_r^{(pl)}$  of the space charge field will be taken into account.

Let us assume that the radial trajectories of electrons do not intersect each other. This means that before the pulse passage, the total charge of electrons,  $Q_e$ , contained initially in a given cross-section in the circle of radius  $r_0$  remains constant:  $Q_e(t) = e\pi r_0^2 n_0 = e\pi r^2(t) n_0$ , where  $n_0$  is the unperturbed plasma density. The total charge of ions contained in the circle of radius  $r(t)$  is  $Q_i = -e\pi n_0 r^2(t)$ . The total charge contained in the circle of radius  $r(t)$  is  $Q_e(t) - Q_i(t) = e\pi n_0 [r_0^2 - r^2(t)]$ . Thus,

$$2\pi r(t) E_r^{(pl)} = 4\pi^2 e n_0 [r_0^2 - r^2(t)]. \quad (7)$$

Here,  $r(t)$  is the trajectory of the electron whose initial radial position is  $r_0$ . The expression for the dimensionless space charge field  $\mathcal{E}_r^{(pl)} = eE_r^{(pl)}/m c \omega$  follows from Eq. (7):

$$\mathcal{E}_r^{(pl)}(\tau) = \frac{\nu^2}{2} \left[ \frac{\rho_0^2}{\rho(\tau)} - \rho(\tau) \right], \quad (8)$$

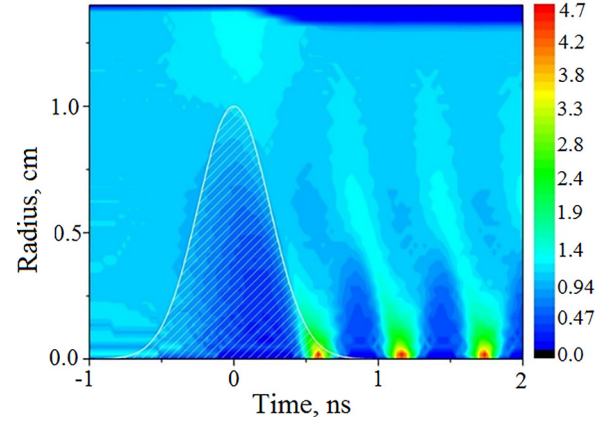


FIG. 1. Evolution of the normalized electron density  $n_e(r, t)/n_0$ . Time  $t = 0$  corresponds to the center of the Gaussian pulse, whose temporal profile is shown as a shaded area.

where  $\nu = \omega_p/\omega \ll 1$ . Equation (6b), in view of Eq. (8), can now be written as

$$\begin{aligned} \frac{d\bar{\beta}_\rho}{d\tau} = & \frac{1}{2} \sin^2\psi \mathcal{E}^2(\bar{\theta}) \left[ \left( \frac{1}{\cos^2\psi} - 2 \right) J_0(\bar{\rho}) + \frac{1}{\rho} J_1(\bar{\rho}) \right] J_1(\bar{\rho}) \\ & + \frac{\nu^2}{2 \sin\psi} \left[ \frac{\rho_0^2}{\rho(\tau)} - \rho(\tau) \right]. \end{aligned} \quad (9)$$

#### V. WAKEFIELD, NUMERICAL SOLUTION

As an example, the temporal evolution of the electron density in a waveguide cross-section, obtained by the numerical solution of Eqs. (6a), (6c), and (6d) and Eq. (9), is presented in Fig. 1. The parameters of the numerical simulation are as follows: the waveguide radius is 1.4 cm, the pulse carrier frequency  $f = 10$  GHz, the plasma density  $n_0 = 3 \times 10^{10} \text{ cm}^{-3}$ , it is assumed that the pulse profile is Gaussian,  $E_0^2(t - z/v_g) \propto \exp[-(t - z/v_g)^2/t_p^2]$ , with  $t_p = 0.35$  ns, and the pulse power 400 MW. It is assumed that the electrons which reach the waveguide wall are absorbed.

The wakefield formation is easily seen in Fig. 1 as a periodic modulation of the electron density after the pulse has left. The period of the modulation is defined by the plasma frequency  $\omega_p$ . Note that the essential radial variation of the plasma density occurs in a region  $\delta r$  of the order of a few mm near the axis, while the axial dimension  $\delta z \approx v_g t_p$  of

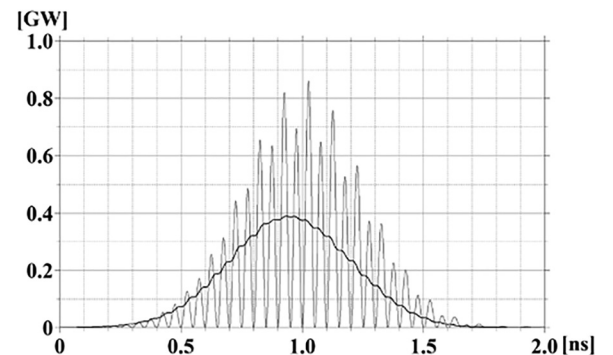


FIG. 2. The shape of a  $\sim 0.85$  GW maximum instantaneous power,  $\bar{P}_{max} = 0.4$  GW average power, 10 GHz frequency, input pulse applied at the upstream boundary of the waveguide.

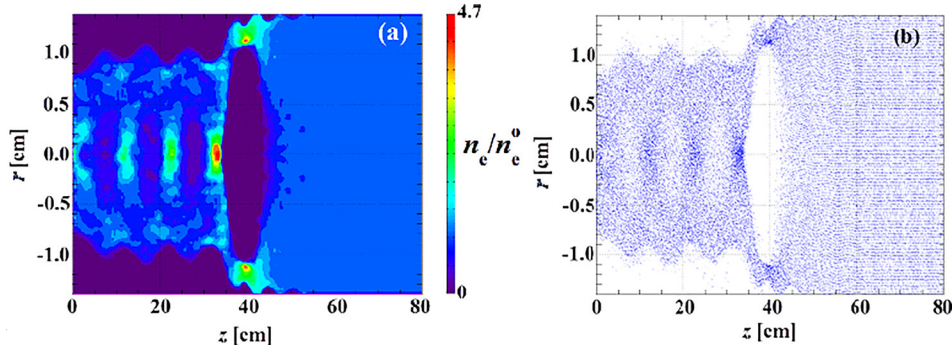


FIG. 3. (a) Relative electron density contours in the  $[r, z]$  plane at  $t = 3.5$  ns. (b) Electron positions at the same time and in the same plane (including all electrons in a 1 mm thick slice for  $\bar{P}_{max} = 0.4$  GW and  $n_e = 3 \times 10^{10} \text{ cm}^{-3}$ ).

this region is of the order of 10 cm. The smallness of the ratio  $\delta r / \delta z \ll 1$  confirms the assumption that the space charge field is directed mainly along the radius.

## VI. PARTICLE IN CELL SIMULATIONS OF THE FORMATION OF A WAKEFIELD IN A PLASMA FILLED WAVEGUIDE

In this section, we present the results of numerical simulations using the 3D Particle in Cell (PIC) code Lsp (Large scale plasma), which implements advanced plasma modeling algorithms,<sup>15,16</sup> for the conditions of the experiments which is being set up in our laboratory. It was shown<sup>5</sup> that when such a microwave pulse is focused by a dielectric lens in an under-dense plasma, a localized wakefield develops at the microwave beam focal waist location with parameters in a region which is simpler to investigate than in the ultra-short high power laser and dense plasma experiments. For these experiments, we are using a super-radiance backward wave oscillator (SRBWO) which produces a  $\text{TM}_{01}$  mode which first converted to a  $\text{TE}_{11}$  mode and then focused to a desired location in the plasma by dielectric lenses.<sup>5</sup>

In the numerical experiments considered here, the high-power microwave  $\text{TM}_{01}$  mode microwave pulses ( $f \approx 10$  GHz, power 0.5–1 GW, pulse duration  $t_p \approx 0.35$  ns at Full Width Half Maximum) generated by the SRBWO are used directly to interact with a preliminarily formed plasma of density  $(2\text{--}5) \times 10^{10} \text{ cm}^{-3}$ . The microwave radiation produced in the corrugated vacuum cylindrical waveguide of the SRBWO is connected at its downstream end to the plasma-filled waveguide of the same radius of 1.4 cm. In the planned

experiments, the plasma will be produced by four flashboard plasma sources<sup>17</sup> placed along the outer walls of a 6.25 cm radius tube, whereas the waveguide consists of 24, 1 mm diameter longitudinal wires uniformly distributed around a transverse 1.45 cm radius circle. This allows sufficient electromagnetic continuity of the waveguide walls. The latter was checked by simulation showing almost 100% efficient microwave pulse propagation inside this cylindrical wire array waveguide. Also, this design enables the plasma to fill the waveguide and the gaps between the wires allow a line of sight for diagnostic observation of the plasma within the waveguide. In contrast to a solid wall waveguide, the plasma electrons can escape through the gaps between the wires.

The simulation model considers an initially formed collisionless plasma of predefined electron density where at each electron position an immobile positive ion is located. We first simulate an 80 cm long and 1.4 cm radius solid conducting waveguide where a  $\text{TM}_{01}$  mode source pulse (see Fig. 2) is applied at its upstream boundary to compare to the analytic predictions described in Secs. IV and V. This pulse propagates along the waveguide and perturbs the stationary electrons in a manner seen in Fig. 3. One can see that when  $\bar{P}_{max} = 0.4$  GW and  $n_e = 3 \times 10^{10} \text{ cm}^{-3}$ , the plasma electrons are *plowed* away by the ponderomotive force from the propagation axis, at first almost completely [Figs. 3(a) and 3(b)] followed by a density wake. This confirms analytical conclusion presented in Secs. III and IV: the radial ponderomotive force is large as compared with longitudinal one and plays the key role in the wakefield formation.

One can see the similarity between Figs. 3(a) and 1, both drawn in the same color scheme and limits of the

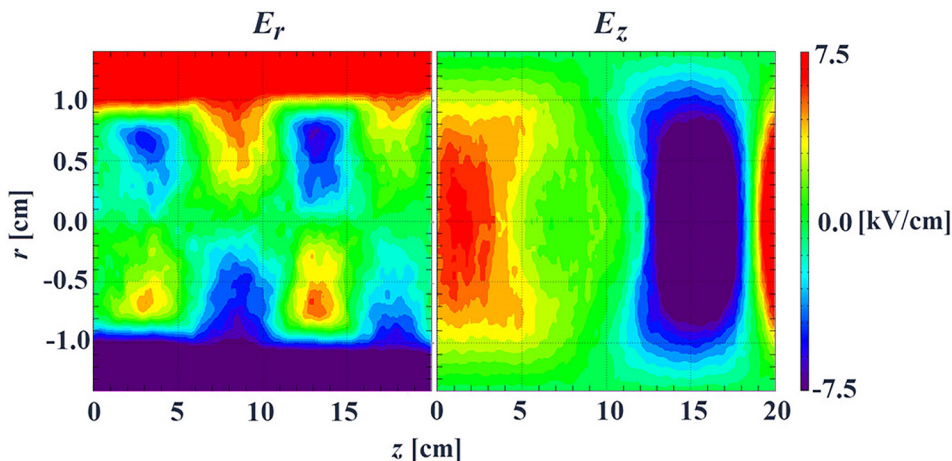


FIG. 4. Contours of  $E_r$  (a) and  $E_z$  (b) in the  $[r, z]$  plane at  $t = 3.5$  ns for the same conditions as those in Fig. 3.

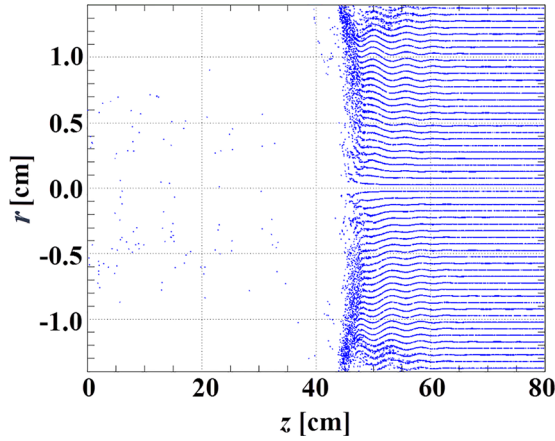


FIG. 5. Electron positions in the  $[r, z]$  plane including all electrons within a 1 mm thick slice, at  $t = 3.5$  ns for  $\bar{P}_{max} = 1.25$  GW and  $n_e = 3 \times 10^{10} \text{ cm}^{-3}$ .

relative density contours. Note in Fig. 3 that  $\delta r$  is of the order of a few mm whereas  $\delta z$  of the order of 10 cm reaffirming the assumptions of the model in Sec. IV, i.e., that the radial electric field of the space charge longitudinal modulation is considerably stronger than the axial one.

In Fig. 4, the  $r$  and  $z$  components of the electric field are drawn at the same time as that in Fig. 3. The contours are drawn in the tail of the wake because in the main further downstream it is difficult to distinguish between the fields of the MW pulse and those of the space charge. Both components are of the same order and relatively weak.

The contour plot in Fig. 4 (right) is split at  $z = 30$  cm into two regions with different contour scales. For  $z > 30$  cm, the propagation of the MW pulse is seen, whereas for  $z < 30$  cm, the much weaker  $E_x$  component of the wakefield appears. The separation of the wakefield from the MW pulse can be deduced from Fig. 4(b).

For large input microwave power ( $\bar{P}_{max} \geq 0.9$  GW), the ponderomotive force at the front of the wave propagating in the waveguide plows almost all electrons to the walls leaving a  $\sim 100\%$  positive ion plasma in the cavity (see Fig. 5). A large volume of positively charged under-dense and low-temperature non-neutral plasma forms this way, which could become an experimental platform for other types of experiments.

The results of simulations of a microwave pulse interacting with the under-dense plasma filling an  $\sim 80$  cm long and 1.4 cm radius waveguide consisting of 24 wires (24W) placed in a conducting tube of 6.25 cm radius representing the experimental setup as explained above are presented next

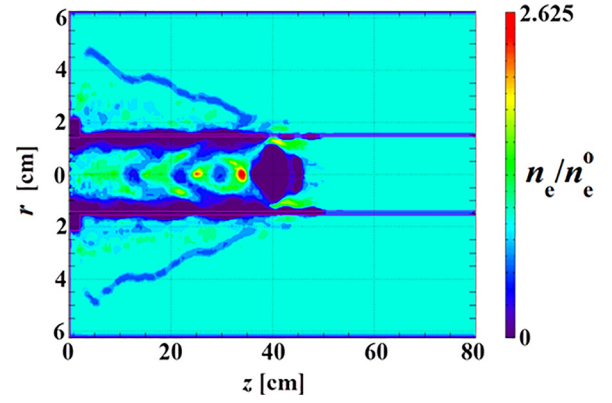


FIG. 6. The same as Fig. 3(a): relative electron density contours in the  $[r, z]$  plane at  $y = 0$  and  $t = 3.5$  ns but for a 1.4 cm radius 24 W waveguide placed in a 6.25 mm radius solid wall waveguide.  $\bar{P}_{max} = 0.4$  GW and  $n_e = 3 \times 10^{10} \text{ cm}^{-3}$ .

in Fig. 6. This is the experimental equivalent of the solid wall waveguide seen in Fig. 3(a).

One can see that as the microwave pulse propagates, the density wake is not limited within the waveguide [Fig. 3(a)] but expands through the gaps between the wires (Fig. 6). This causes the wake inside the waveguide to decay and more difficult for experimental detection. Using the data presented in Fig. 6, one can estimate the energy  $W_e$  of electrons escaping the wire array waveguide as  $W_e \approx 0.9$  keV.

One can constrain the plasma electrons within the 24 W waveguide by applying an external axial magnetic field,  $B_z$ .<sup>18</sup> In Fig. 7(a), one can see that a relatively small  $B_z = 500$  G is sufficient to contain the electrons within the waveguide and sustain a wake. The wake is completely suppressed for a stronger magnetic field due to electron magnetization.

Finally, in Fig. 7(b), one can see the plasma density modulations when in addition to applying a uniform axial magnetic field of 500 G, the 24 W waveguide was closed with a downstream conducting endplate. The latter results in reflected electromagnetic waves, leading to the appearance of a delayed second strong plasma density modulation. The wake is though weakened because of interference between the forward and backward wakes.

## VII. CONCLUSIONS

Analytical modeling and PIC simulations showed the feasibility of excitation of a large scale spatial wakefield by a short high-power microwave pulse propagating in a cylindrical waveguide filled with under-dense plasma. Depending on the parameters of the plasma and microwave power,

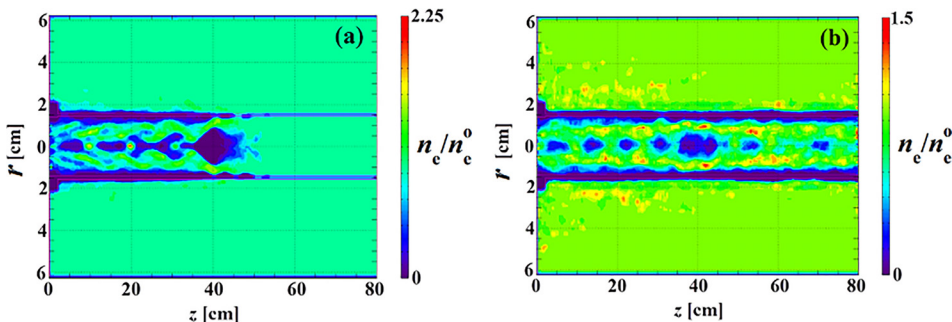


FIG. 7. The same as Fig. 5 but (a) with an applied external  $B_z = 500$  G ( $t = 3.5$  ns) and (b) with a conducting endplate at  $z = 80$  cm ( $t = 8.4$  ns).

almost 100% density modulation can be obtained. It is shown that the TM mode of circular waveguide produces mainly radial ponderomotive force which exceeds considerably the longitudinal one.

## ACKNOWLEDGMENTS

The authors are grateful to Dale Welch and Chris Mostrom of Voss Scientific Inc. for their assistance in setting up and running Lsp. This work was supported in part by the PAZY Grant No. #2020960 and by the Center for Absorption in Science, Ministry of Immigrant Absorption, State of Israel.

<sup>1</sup>T. Tajima and J. Dawson, *Phys. Rev. Lett.* **43**, 267 (1979).

<sup>2</sup>E. Esarey, C. Schroeder, and W. Leemans, *Rev. Mod. Phys.* **81**, 1229 (2009).

<sup>3</sup>V. Malka, *Phys. Plasmas* **19**, 55501 (2012).

<sup>4</sup>W. P. Leemans, B. Nagler, A. J. Gonsalves, C. Tóth, K. Nakamura, C. G. R. Geddes, E. Esarey, C. B. Schroeder, and S. M. Hooker, *Nat. Phys.* **2**, 696 (2006).

<sup>5</sup>G. Shafir, A. Shlapakovski, M. Siman-Tov, Y. Bliokh, J. G. Leopold, S. Gleizer, R. Gad, V. V. Rostov, and Y. E. Krasik, *J. Appl. Phys.* **121**, 033301 (2017).

<sup>6</sup>V. V. Rostov, I. V. Romanchenko, M. S. Pedos, and M. I. Yalandin, *Phys. Plasmas* **23**, 093103 (2016).

<sup>7</sup>H. K. Malik, *J. Appl. Phys.* **104**, 053308 (2008).

<sup>8</sup>S. K. Tomar and H. K. Malik, *Phys. Plasmas* **20**, 072101 (2013).

<sup>9</sup>H. K. Malik and A. K. Aria, *J. Appl. Phys.* **108**, 013109 (2010).

<sup>10</sup>H. K. Malik and S. Kumar, *Laser Part. Beams* **26**, 197 (2008).

<sup>11</sup>A. K. Aria and H. K. Malik, *Open Plasma Phys. J.* **1**, 1 (2008).

<sup>12</sup>A. K. Aria and H. K. Malik, *Opt. Commun.* **282**, 423 (2009).

<sup>13</sup>N. S. Ginzburg, N. Y. Novozhilova, I. V. Zotova, A. S. Sergeev, N. Y. Peskov, A. D. Phelps, S. M. Wiggins, A. W. Cross, K. Ronald, W. He, V. G. Shpak, M. I. Yalandin, S. A. Shunailov, M. R. Ulmaskulov, and V. P. Tarakanov, *Phys. Rev. E* **60**, 3297 (1999).

<sup>14</sup>A. A. Eltchaninov, S. D. Korovin, V. V. Rostov, I. V. Pegel, G. A. Mesyats, S. N. Rukin, V. G. Shpak, M. I. Yalandin, and N. S. Ginzburg, *Laser Part. Beams* **21**, 187 (2003).

<sup>15</sup>D. R. Welch, D. V. Rose, B. V. Oliver, and R. E. Clark, *Nucl. Instrum. Methods Phys. Res., Sect. A* **464**, 134 (2001).

<sup>16</sup>D. R. Welch, D. V. Rose, M. E. Cuneo, R. B. Campbell, and T. A. Mehlhorn, *Phys. Plasmas* **13**, 063105 (2006).

<sup>17</sup>T. J. Renk, *J. Appl. Phys.* **65**, 2652 (1989).

<sup>18</sup>G. Brodin and J. Lundberg, *Phys. Rev. E* **57**, 7041 (1998).